Steel and Composite Structures, Vol. 2, No. 6 (2002) 441-460
DOI: http://dx.doi.org/10.12989/scs.2002.2.6.441

Design thermal loading for composite bridges in tropical region

F.T.K. Au†, S.K. Cheung†† and L.G. Tham‡†

Department of Civil Engineering, The University of Hong Kong, Pokfulam Road, Hong Kong, China

(Received June 5, 2002, Accepted November 8, 2002)

Abstract. In the design of bridges, it is important to consider the thermal stresses induced by the non-linear temperature distribution as well as the variation of effective temperature in the bridge deck. To cope with this, design temperature profiles are provided by design codes, which are normally based on extensive research work. This paper presents the results of a comprehensive investigation on the thermal behaviour of bridges in Hong Kong with special emphasis on composite bridges. The temperature distribution in bridges depends primarily on the solar radiation, ambient air temperature and wind speed in the vicinity. Apart from data of the meteorological factors, good estimates of the thermal properties of material and the film coefficients are necessary for the prediction of temperature distribution. The design temperature profiles for various types of composite bridge deck with bituminous surfacing and concrete slab of different thicknesses are proposed. The factors affecting the design effective temperature are also reviewed and suitable values for Hong Kong are proposed. Results are compared with recommendations of the current local code. The method facilitates the development of site-specific temperature profiles for code documents, and it can also be applied to create zoning maps for temperature loading for large countries where there are great climatic differences.

Keywords: composite bridge; extreme analysis; temperature; temperature gradient; thermal response.

1. Introduction

It has long been recognised that the temperature in bridge decks varies with the external environment. Apart from the overall movement and deformation of bridge decks in response to changes in the effective bridge temperature, stresses are set up due to changes in temperature gradient within the cross section. Such thermal loading influences not only the design of movement joints and bridge bearings, but also the bridge decks, bridge piers and other structural elements. Overlooking the effects of such repeated cycles of heating and cooling might give rise to distress in various parts of the structure.

Researchers such as Zuk (1965) began to study the thermal behaviour of highway bridges since 1960. From a number of bridges investigated, it was concluded that the air temperature, wind, humidity, intensity of solar radiation and material type would all affect the temperature distribution. On that basis, Reynolds and Emanuel (1974) further investigated the properties of the temperature differential and the

†Associate Professor
††Part-time M.Sc.(Eng.) student
‡†Senior Lecturer

effect of asphalt surfacing. Subsequent research work on the topic mainly concentrated on the prediction of temperature distribution for different forms of bridges. They included the work on steel decks by Capps (1968), concrete deck by Hunt and Cooke (1975) and composite deck by Emerson (1973) as well as Kennedy and Soliman (1987).

2. Review of design codes

Investigations in the thermal behaviour of bridges in the U.K. were primarily carried out by the Transport and Road Research Laboratory (TRRL). Emerson (1973) reported that the temperature distribution down the depth was non-linear, which implies that thermal stresses will always be induced whether the structure is simply supported or continuous. In addition, the TRRL also studied the thermal movements as well as the estimation of temperature distribution from the shade temperature (Capps 1968, Emerson 1968, Emerson 1976). The code BS5400 (BSI 1978) encompassing the design of steel, concrete and composite bridges was introduced in 1978. The part on thermal loading was actually drafted on the basis of the findings of the TRRL.

However, as climatic conditions differ, the conclusions and design rules drawn up for one country could not be applied generally, without modification, in another. In view of this, various programmes on the measurements of temperature distributions in highway bridges were initiated by the Highways Department (HyD) of the Hong Kong Government starting from 1980. The Castle Peak/ Texaco Road Flyover and the Cornwall Road/ Waterloo Road/ Junction Road Interchange have been studied in detail (Liu 1985, Ho and Liu 1989). These findings were extensively used in the local design codes such as the currently used Structures Design Manual for Highways and Railways (SDMHR) (HyD 1997). The relevant section of the local code on thermal loading has been written generally in line with the British code, except that certain parameters have been adjusted to account for the local climatic conditions. Depending on the type of construction, bridge decks are divided into four groups, namely steel deck on steel box girder (Type 1), steel deck on steel truss or plate girder (Type 2), concrete deck on steel box, truss or plate girders (Type 3), and concrete slab and concrete beam-and-slab deck (Type 4). Effective bridge temperatures and temperature differences are specified for various groups of structures. The necessary adjustments for thickness of surfacing and height above mean sea level are also specified. However these recommendations have been drafted on the basis of field measurements in concrete bridges only.

Different approaches have been adopted for the specification of thermal loading for bridges in different countries. In the United States, detailed specification of the positive and reverse temperature gradients are given for concrete and composite bridges by the AASHTO Code (AASHTO 1998). However, only the extreme effective bridge temperatures are given for steel bridges (AASHTO 1996). This is probably due to the smaller temperature gradients caused by the higher thermal conductivity of steel. Investigations in New Zealand were mainly focused on the temperature-depth relationship within the bridge deck. Priestley (1978) proposed a non-linear distribution represented by a fifth-order polynomial at the top, a uniform segment in the middle and a linear distribution at the bottom. In Canada, the Ontario Highway Bridge Design Code (OHBDC) (Ministry of Transport, Canada, 1991) specifies the effective temperature for different types of bridges. Apart from that, an effective construction temperature of 15°C is also assumed in the calculation of thermal expansion and contraction.

3. Investigations by scale models

The most ideal method of investigation is to instrument prototype bridges for temperature monitoring. However, for various practical reasons, it may not be possible to put instrumentation in all the components of interest. For example, trough stiffeners and box girders cannot normally be drilled through; otherwise the warranty will become void. It is therefore necessary to complement such on site monitoring of actual structures with experiments on scale models. Three steel segmental models (Fig. 1) with instrumentation have been set up on the roof of a building on the campus of the University of Hong Kong since 1993 (Au *et al.* 1999).

The models include two box girder sections and a plate girder section, all of which have been fabricated from steel plates. Both box girder sections have cross sectional dimensions of 624 mm×396 mm. One of them has the ends open so that the cell is freely ventilated while the other has both ends blocked by plywood to simulate normal box girders in which the interior is not freely ventilated. The plate girder section comprises a 1600 mm wide steel plate supported on two I-beam sections of 800 mm depth. Platinum resistance type detectors are used to measure temperatures of the steel plates and shade temperatures at various locations. 15 channels are provided on each box girder model and 18 channels are provided on the plate girder section. Measurements are taken and stored by data loggers at half-hour intervals. Data retrieval is then done by a notebook computer every fortnight.

Statistical correlation was carried out between the field measurements and the meteorological data given by the Hong Kong Observatory (Au *et al.* 1999). It shows that the daily maximum temperature of the bridge deck depends on both the daily maximum air temperature and the global solar radiation. From the multiple linear correlations done on the data from July 1994 to December 1998, a correlation coefficient larger than 0.82 was obtained. However, the daily minimum temperature of the bridge deck was shown to correlate with the daily minimum air temperature only, and a correlation coefficient larger than 0.90 was obtained from simple linear correlation.

Hourly global solar radiation data are available from the Hong Kong Observatory. They represent the total effect of direct and diffuse solar radiation on a horizontal surface. However similar data on surfaces of different orientations need to be calculated and the approach suggested by Yik *et al.* (1995) has been adopted. From previous work carried out in the 1980s (Liu 1985, Ho and Liu 1989), it is

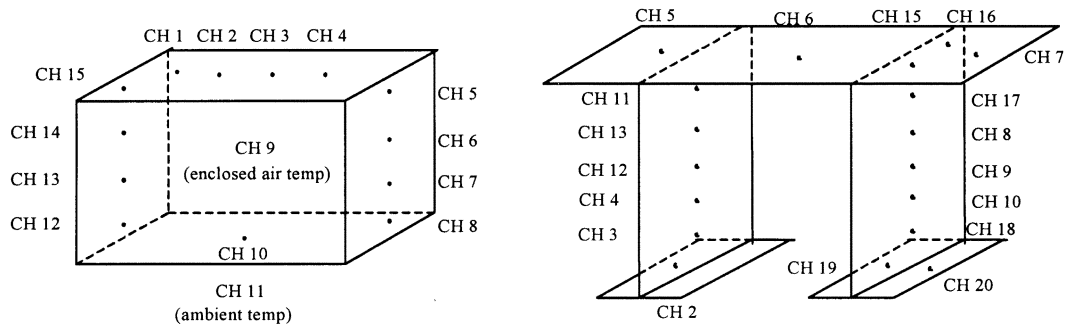

(a) Box girder section. (b) Plate girder section.

Fig. 1 Scaled models used in investigation

evident that the cooling of the bridge deck at night also depends on the outgoing radiation. Similar rationale was followed to formulate the outgoing radiation at night.

4. Theoretical background

The thermal behaviour of a bridge section is generally governed by the meteorological factors and the properties of construction materials of the bridge. Among various meteorological factors, the ambient air temperature and the intensity of solar radiation have been shown to be influential. The temperature distribution at a section is normally described by its effective temperature and the temperature difference there. The effective temperature is the weighted mean value of temperature at the section defined as

$$T_e = \int E\alpha T dA / \int E\alpha dA \tag{1}$$

where E is the Young's modulus, α is the coefficient of thermal expansion, T is the temperature, dA is the differential cross-sectional area, and integration is carried out over the whole cross section.

The temperature difference refers to the difference in temperature from that at a chosen reference point in the section. The daily extreme air temperatures usually affect the effective temperature while the solar radiation usually contributes to the temperature difference in the section. The overall expansion of the bridge deck can be calculated from the product of the change in effective temperature, the coefficient of thermal expansion and the total length. If the deck were restrained, the temperature difference would tend to induce a bending moment given by

$$M_0 = \int E\alpha T y dA \tag{2}$$

where y is the distance from the horizontal centroidal axis of the section. Stresses may be induced depending on the ability of the structure to deform.

Since the effect of temperature gradient on the structural behaviour is considerable, the prediction of this gradient in different structures according to the local meteorological condition becomes essential. The temperature distribution within a section is governed by heat conduction inside its body, and the convective and radiative heat exchange with the surrounding environment. Under normal circumstances, the longitudinal heat flow in a prismatic section can be neglected. Because of the high thermal conductivity and small thickness of steel plate, the temperature gradient across the thickness is neglected. Therefore, conductive heat flow is only considered along the width of each steel plate. For the modelling of the concrete slab, a simplified finite element mesh simulating the two-dimensional heat flow is adopted. Heat exchange with surrounding through convection and radiation takes place on the two surfaces only. The transient one-dimensional heat flow by conduction in a homogeneous solid follows Fourier's law

$$k\frac{\partial^2 T}{\partial x^2} = \rho c \frac{\partial T}{\partial t} \tag{3}$$

where k is the thermal conductivity, ρ is the density, c is the specific heat capacity, and T is the temperature at position x at time t. At the interface with surrounding, the heat flow relationship with

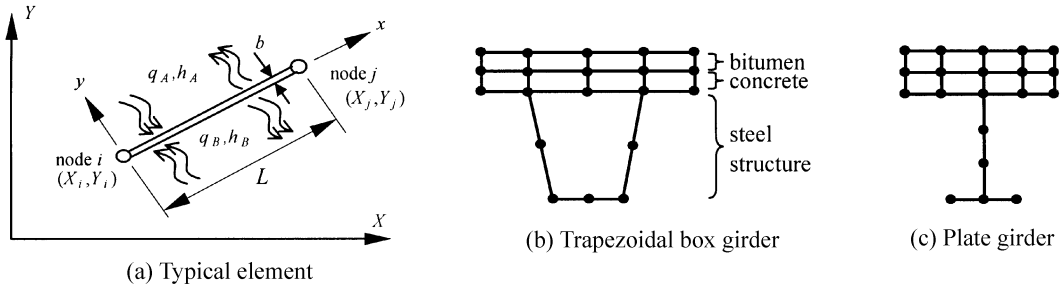

(a) Typical element

(b) Trapezoidal box girder

(c) Plate girder

Fig. 2 Finite element models

convection and radiation during daytime is given by

$$-k\frac{\partial T}{\partial n}-h(T-T_a)+\alpha I = 0 \tag{4}$$

where h is the film coefficient, T_a is the ambient temperature, α is the absorptivity, I is the solar intensity, and n is the normal to the surface. A similar equation at night when there is outgoing radiation emitted from the bridge can be written, and it depends on the emissivity of the surface ξ.

To apply the above theory to the bridge section, the section is discretized into elements as shown in Fig. 2. Note that the concrete slab is modelled as a grillage of similar elements for convenience. This is already better than the finite difference method adopted by the previous work on concrete bridges (Liu 1985, Ho and Liu 1989). Based on the variational approach, the equation governing heat transfer can be written as

$$\left(\frac{kb}{L}\begin{bmatrix}1 & -1\\ -1 & 1\end{bmatrix}+\frac{1}{6}L(h_a+h_b)\begin{bmatrix}2 & 1\\ 1 & 2\end{bmatrix}\right)\{T\}+\left(\frac{1}{6}bL\rho c\begin{bmatrix}2 & 1\\ 1 & 2\end{bmatrix}\right)\{\dot{T}\}$$
$$=-\frac{1}{2}L(q_a+q_b)\begin{Bmatrix}1\\ 1\end{Bmatrix}+\frac{1}{2}L(h_a(T_a)_a+h_b(T_a)_b)\begin{Bmatrix}1\\ 1\end{Bmatrix} \tag{5}$$

where b and L are the thickness and length of the element respectively. Note that the subscripts a and b correspond to sides A and B of the element respectively.

Following the standard finite element procedure, one can easily assemble the characteristic matrices and solve for the temperature distribution of the section by carrying out forward time marching (Tong *et al.* 2001). In the analysis, a number of parameters are required. The density ρ, the specific heat capacity c and the thermal conductivity k are known fairly accurately. However, the film coefficients and heat flux depend on the environment and may not be readily available. The film coefficient h at a surface represents the total amount of thermal energy lost per unit area to the surrounding caused by a unit temperature difference between the surface and the surrounding. Thermal energy is lost to the surrounding at different rates by natural convection, forced convection and radiation. Each kind of heat exchange would be governed by its own heat transfer coefficient. For simplicity, various researchers (Capps 1968, Emerson 1973, Liu 1985, Tong 2000) have combined the heat losses by convection and radiation, and generated the film coefficient h that governs the total effect of heat loss. It was shown by these researchers that the film coefficient varies from 2 W/K/m^2 to 23 W/K/m^2 depending on wind

Table 1 Initial parameters adopted in the investigation using scale model

	Tong (2000)	Capps (1968)	Hirst (1981)
Density ρ (kg/m^3)	7854	7818	7900
Specific heat capacity c (J/kg/K)	434	460	460
Thermal conductivity k (W/m/K)	60.5	-	47
Film coefficient at top h_{a1} (W/m^2/K)	16.5	17.7	11+1.2v
File coefficient at bottom h_{a2} (W/m^2/K)	5	8.5	9
Film coefficient of air void h_b (W/m^2/K)	1	1.6	-
Absorptivity α	0.5	0.88	-
Emissivity ξ	0.5	0.88	-

Note: v is the wind speed in m/s.

Table 2 Comparison of initial and adjusted parameters for model investigation

	Initial	Open box (adjusted)	Plate girder (adjusted)
Film coefficient at top h_{a1} (W/m^2/K)	16.5	21.5	15.2
File coefficient at bottom h_{a2} (W/m^2/K)	5	23.5	1.62
Film coefficient of air void h_b (W/m^2/K)	1	1.5	-
Absorptivity α	0.5	0.48	0.48
Emissivity ξ	0.5	0.52	0.61

speed, location and orientation of the surface. These values may be used in the analysis but it may be necessary to carry out a parametric search to establish the best values for the given environmental conditions. Table 1 shows the initial parameters adopted for the study carried out by Tong (2000) compared with those adopted by Capps (1968) and Hirst (1981). The absorptivity α and the emissivity ξ are less certain and they depend on the surface texture and colour. Sensitivity analyses have been carried out, and these parameters are adjusted. A comparison of the initial and adjusted values is shown in Table 2.

5. Field study and calibration of numerical model

Before the methodology developed at the model investigations can be generally applied to real life situations, it is necessary to test it with actual structures. Tong *et al.* (2000) reported some results of the temperature measurements taken at various superstructure components of Tsing Ma Bridge, a suspension bridge in Hong Kong having a steel deck. A continuous 30-month temperature record on Tsing Ma Bridge up to December 1999 has been used as a database for the investigation, and hourly global solar radiation data are provided by the Hong Kong Observatory. The data have been analysed and various numerical models have been set up and calibrated against the field data. In particular, the meteorological conditions on one summer day (4 August 1998) and one winter day (17 January 1998) have been chosen for analysis and comparison with field measurements. Similar to the previous study on segmental steel box sections, the values for film coefficients, absorptivity and emissivity have been worked out after a series of parametric studies. The validity of the one-dimensional temperature profile is also confirmed.

The present study focuses on composite bridge decks with or without bituminous surfacing, which

Table 3 Parameters adopted in the present study

		Steel	Concrete	Asphalt
Density (kg/m^3)		7854	2450	2100
Specific Heat Capacity (J/kg/K)		434	763	840
Thermal conductivity (W/m/K)		60.5	1.82	0.7
Absorptivity		-	(0.65)	0.9
Emissivity		-	(0.9)	0.9
Film coefficient (W/m^2/K)	(Upward heat loss)		17.5	
	(Downward heat loss)		6.8	

Note: Values within brackets are for bare concrete surfaces.

comprises a concrete slab supported on steel girders. The parameters adopted in the present study consist of the thermal properties of concrete validated by Liu (1985), and the properties of asphalt and steel in the study on steel bridges (Tong 2000). These parameters are summarized in Table 3.

6. Parametric studies for determination of design thermal loading

A number of composite bridge sections have been studied (Cheung 2002) following the approach adopted by Au *et al.* (2001) for steel bridges. They are (a) plate girders, (b) trapezoidal box girders, and (c) rectangular box girders, as shown in Fig. 3. From the study, it is found that the plate girders and the trapezoidal box girders produce the steepest temperature gradient in the steel web as well as the highest effective temperature. Therefore they are chosen for the subsequent analysis, and hereafter a box girder section refers to the trapezoidal box girder section (Fig. 3b) unless otherwise stated.

Fig. 3 also shows the notations and default dimensions of the plate girder and the box girder chosen for parametric studies. The section depth d_l is taken as 1000 mm so as to allow sufficient depth for the girder web to return to the ambient air temperature. The meteorological conditions of the chosen summer day are assumed, and the solar radiation is taken to act only on the top surface of the top flange.

Strictly speaking the temperature distribution of a composite bridge deck depends on all the geometric and material parameters in addition to the environment. However most design codes classify sections into categories, each of which has one single design profile. The thermal properties of steel,

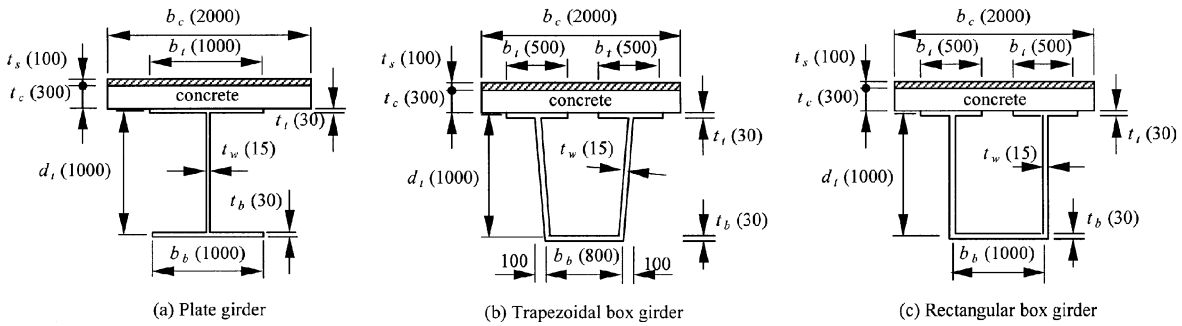

Fig. 3 Sections adopted in sensitivity studies and extreme analysis, with default dimensions in mm (not to scale)

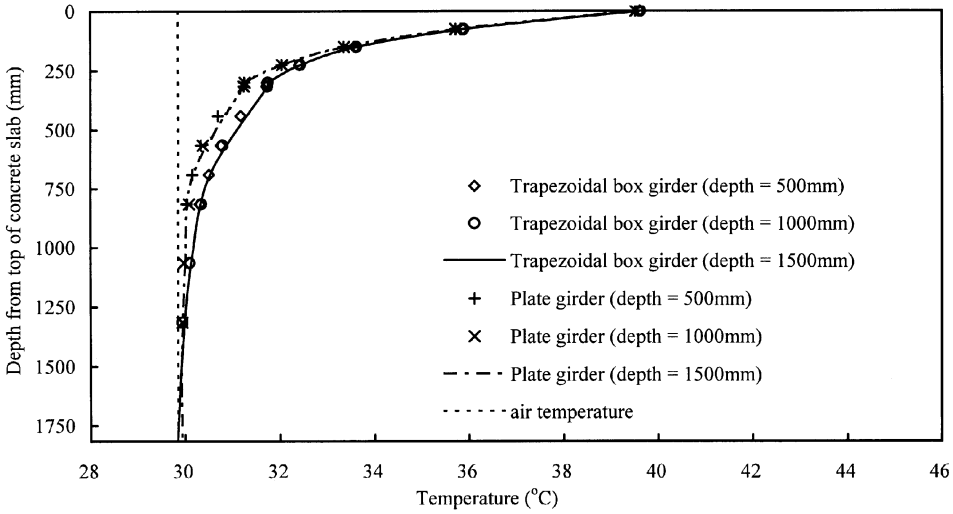

Fig. 4 Effects of section depth on temperature profile

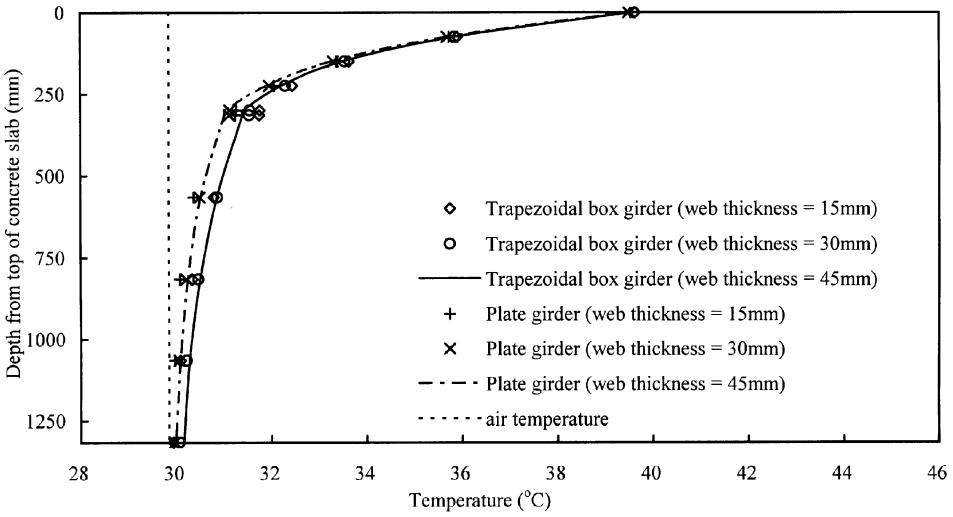

Fig. 5 Effects of web thickness on temperature profile

concrete and bituminous surfacing are known with little uncertainty. A study on the influence of geometric parameters on the temperature distribution of composite sections has been carried out (Cheung 2002) by varying only a parameter each time. For example, to investigate the effects of section depth d_t, it is varied from 500 mm to 1500 mm, while the other dimensions are the same as those shown in Fig. 3 unless otherwise noted hereafter. Fig. 4 shows that the temperature profiles are not sensitive to the total girder depth. Similarly the effects of girder spacing b_t on the temperature profile are studied and found to be minimal for both sections. The temperatures at the flanges are also found to be relatively constant across the width. The effects of web thickness t_w on the temperature profiles are studied by varying t_w from 15 mm to 45 mm. Fig. 5 shows that increasing the web thickness does reduce the temperature gradient a bit. Adopting the temperature profiles for a thin web of 15 mm is a

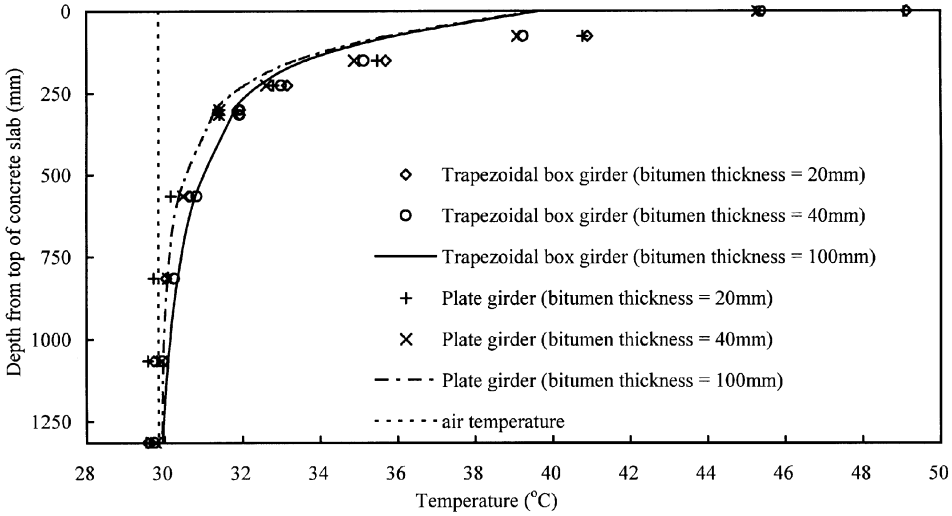

Fig. 6 Effects of bitumen thickness on temperature profile

reasonable approach on the safe side. The effects of top flange thickness t_t on the temperature profiles are likewise studied. The effects are similar to those caused by the variation of web thickness. The thickness of bituminous surfacing t_s is varied from 20 mm to 100 mm for both sections. The effects as shown in Fig. 6 are substantial. The deck surface temperature increases as the thickness of bituminous surfacing reduces. In a similar fashion, the thickness of concrete slab t_c is varied from 150 mm to 450 mm for both sections. The effects as shown in Fig. 7 are also significant. The temperature gradient in the steel web increases as the concrete slab becomes thinner. The effects of top flange width b_t on the temperature profiles are studied by varying b_t from 100 mm to 900 mm for the box girder and 200 mm to 1800 mm for the plate girder. Fig. 8 shows that the effects are not obvious. Therefore for practical

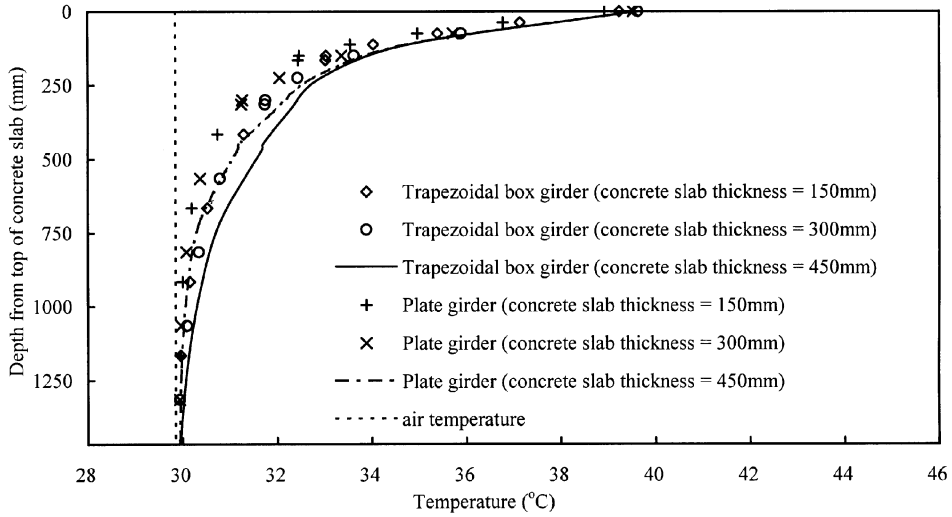

Fig. 7 Effects of concrete thickness on temperature profile

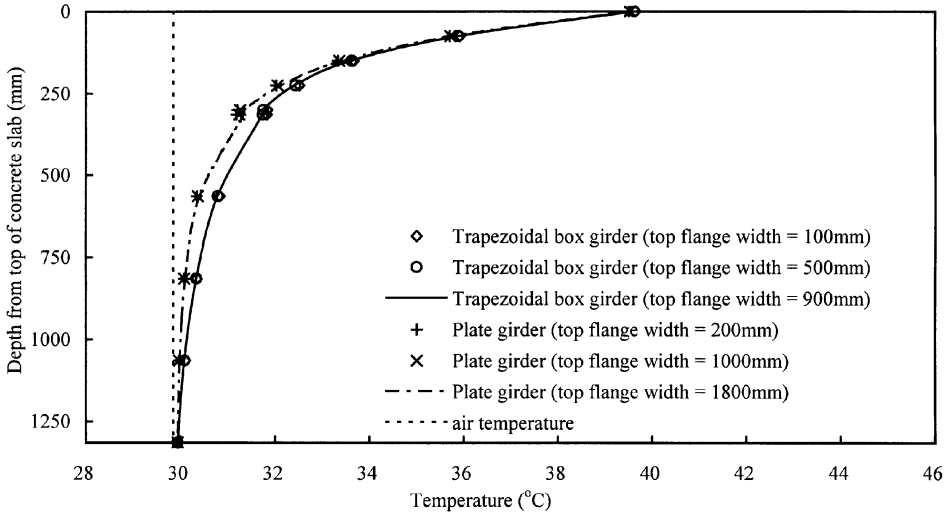

Fig. 8 Effects of top flange width on temperature profile

design purposes, the effects caused by changes in girder depth, girder spacing, web thickness, flange thickness and top flange width are minimal. The only significant factors are the thicknesses of the bituminous surfacing and concrete slab.

A study on the transverse variation of temperature in the concrete slab and the top steel flange of the girder is also carried out. Two plate girder sections as shown in Fig. 3 with concrete slab thicknesses of 150 mm and 300 mm are analysed under the meteorological conditions of the chosen summer day. Fig. 9 shows the temperature at the mid-plane of the concrete slab and the top steel flange of the plate girders. The results reveal that the transverse variation of temperature reduces with increasing slab thickness. In all cases investigated, the transverse variation of temperature is below 1°C. It shows that

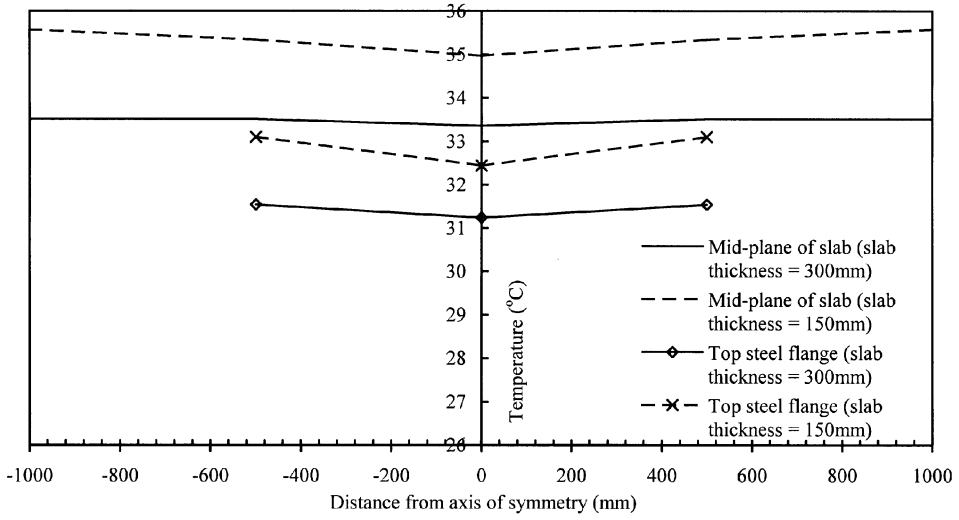

Fig. 9 Transverse variation of temperature in concrete slab and top steel flange

the use of a representative temperature profile along the web plane while ignoring any transverse temperature variation is acceptable.

7. Extreme distributions of climatic factors

The thermal loads on a bridge may be considered as random functions of the random variables T_{max}, the daily maximum air temperature, T_{min}, the daily minimum air temperature and Q, the daily global solar radiation. The extreme thermal loads are therefore random variables. To predict the probability of occurrence of their maxima and minima, their frequency distributions are required. It is assumed that the extreme thermal loads are functions of the extreme values of Q and T_{max}.

To determine the extreme thermal loads at a geographical location, it is necessary to carry out the extreme analysis of the climatic factors first. Gumbel (1960) has observed that the tails of the frequency distributions of most climatic factors decay in an exponential manner. Among n observations of a random variable y, the cumulative distribution function of the largest value Y_n follows a double-exponential Type I asymptotic distributions, namely

$$P_{Y_n}(y) = \text{Prob}(Y_n < y) = \exp[-e^{-a_n(y-u_n)}] \tag{6}$$

where a_n is the scale parameter and u_n is the location parameter. When the above extreme distribution is defined, the design value for any return period can be calculated from the statistics of extremes. In the study, the parameters a_n and u_n are obtained from the linearised plot of the climatic factor y_i from n observations and their corresponding probabilities p_i using the reduced variate x_i, defined as (Ho and Liu 1989):

$$x = -\ln[-\ln(P_{Y_n}(y))] \tag{7}$$

Therefore x_i and y_i are related by

$$x = a_n(y - u_n) \tag{8}$$

The corresponding cumulative distribution function for the smallest value Y_1 among the n observed values is

$$P_{Y_1}(y) = \text{Prob}(Y_1 < y) = 1 - \exp[-e^{-a_1(y-u_1)}] \tag{9}$$

and x_i and y_i are similarly related by

$$x = a_1(y - u_1) \tag{10}$$

Statistical analyses are carried out based on the meteorological records of the Hong Kong Observatory since 1958. Table 4 summarizes the statistics of climatic factors adopted (Tong 2000) together with the predicted values y_{50} and y_{120} for return periods of 50 and 120 years respectively.

To facilitate subsequent extreme analysis of thermal loading, it is useful to adopt equations to express the instantaneous values of climatic factors in terms of their extreme values. The adopted expression for

Table 4 Statistics and predicted values of climatic factors obtained by Tong (2000)

	a_n or a_1	u_n or u_1	Statistics					
			μ	σ	θ	κ	y_{50}	y_{120}
Daily maximum air temperature (°C)	1.6	34.0	34.33	0.78	1.14	5.40	36.4	36.9
Daily minimum air temperature (°C)	-0.7	7.5	6.74	1.76	-1.14	5.40	2.2	1.0
Max. global solar radiation (MJ/m^2/day)	0.5	26.2	27.43	2.81	1.14	5.40	34.7	36.7

the instantaneous solar intensity I_t is due to Hirst (1981), namely

$$I_t = (2I_{DG}/D)\cdot \sin^2(\pi t_{sol}/D) \tag{11}$$

where I_{DG} is the daily global solar radiation, D is the length of solar daytime and t_{sol} is the solar time. The expression adopted for the diurnal variation of air temperature T_a has been determined by curve fitting from local meteorological records (Ho and Liu 1989) as

$$T_a(t) = \begin{cases} (T_{\max}+T_{\min})/2-(t+6)(T_{\max}-T_{\min})/24 & 0 \le t<6 \\ (T_{\max}+T_{\min})/2-\sin[\pi(t-10)/8](T_{\max}-T_{\min})/2 & 6 \le t<18 \\ (T_{\max}+T_{\min})/2-(t-18)(T_{\max}-T_{\min})/24 & 18 \le t<24 \end{cases} \tag{12}$$

where t is local time in hours. Based on regression of the local meteorological records from 1997 to 1999, the daily maximum and minimum air temperatures for summer and winter are given respectively by

$$T_{\min} = 0.46T_{\max}+7.46 \qquad \text{for summer} \tag{13}$$

$$T_{\max} = 0.96T_{\min}+4.76 \qquad \text{for winter} \tag{14}$$

To predict the extreme positive temperature gradient in summer, the extreme value of daily global solar radiation Q is used. In addition, the diurnal variation of air temperature T_a is assumed to follow Eq. (12) using the extreme value of daily maximum air temperature $T_{\max}$ and the daily minimum air temperature $T_{\min}$ given by Eq. (13). To predict the extreme reverse temperature gradient during a winter night, the diurnal variation of air temperature T_a is similarly based on the extreme value of daily minimum air temperature $T_{\min}$ and the daily maximum air temperature $T_{\max}$ given by Eq. (14). The variation of out-going radiation is assumed to take a trapezoidal profile (Tong 2000). It increases linearly from zero at 20:00 to 85.3 W/m^2 at 23:00, remaining constant at 85.3 W/m^2 until 3:00 the following day, and then decreases linearly from 85.3 W/m^2 to zero at 6:00. The predicted results based on this compare favourably with field measurements.

8. Extreme distributions of thermal loading

Theoretically, the extreme distributions of bridge thermal loading can be evaluated in a similar manner as the climatic factors. However, this approach requires a database with long period of field

measurements, which is not available. A convenient, though not mathematically rigorous, alternative is to evaluate the extreme thermal loading by using numerical integration (Ho and Liu 1989). Firstly the statistical parameters, including the mean μ, standard deviation σ, skewness θ and kurtosis κ, which define the extreme distributions of air temperature and solar radiation are calculated. The statistical parameters of the reduced variate x of the double-exponential Type I asymptotic distributions described by Eq. (6) are given by Gumbel (1960) as $\mu_x = 0.57722$, $\sigma_x = 1.28255$, $\theta_x = 1.13955$ and $\kappa_x = 5.40$. For the largest value of each climatic factor, the statistical parameters are related to a_n and u_n by $\mu_y = 0.57722/a_n + u_n$, $\sigma_y = 1.28255/a_n$, $\theta_y = 1.13955$ and $\kappa_y = 5.40$. The corresponding statistical parameters for the smallest value are $\mu_y = 0.57722/a_1 + u_1$, $\sigma_y = -1.28255/a_1$, $\theta_y = -1.13955$ and $\kappa_y = 5.40$.

The statistical modelling by numerical integration technique suggested by Evans (1972) and subsequently modified by Ho and Liu (1989) is used here. Let $f(x)$ be a random function of a random variable x. Supposing the frequency distribution of x is given by $p(x)$, then the expectation of $f(x)$ is given by Gaussian quadrature with three Gaussian points as

$$E(f) = \int_{-\infty}^{\infty} p(x)f(x)dx = \mu \cong \sum_{i=1}^{3} A_i f(x_i) \tag{15}$$

where A_i is the weighting coefficient associated with the position of Gaussian point x_i as given explicitly by Ho and Liu (1989).

Similarly, for a random function $g(x, y)$ of two independent random variables x and y with their respective frequency distributions $p_1(x)$ and $p_2(y)$, the expectation $E(g)$ of $g(x, y)$ is given by Ho and Liu (1989) as:

$$E(g) = \int_{-\infty}^{\infty}\int_{-\infty}^{\infty} p_1(x)p_2(y)g(x,y)dxdy = \int_{-\infty}^{\infty} p_1(x)\left(\int_{-\infty}^{\infty} p_2(y)g(x,y)dy\right)dx \tag{16}$$

The parameters x_i and A_i for Guassian quadrature in the x direction and the parameters y_j and B_j in the y direction can be similarly determined (Ho and Liu 1989). Then the mean μ_g, standard deviation σ_g, skewness θ_g and kurtosis κ_g of the function $g(x, y)$ become

$$\mu_g = \sum_{i=1}^{3}\sum_{j=1}^{3} A_i B_j g(x_i, y_j) \tag{17}$$

$$\sigma_g = \sqrt{\sum_{i=1}^{3}\sum_{j=1}^{3} A_i B_j [g(x_i, y_j) - \mu_g]^2} \tag{18}$$

$$\theta_g = \frac{1}{\sigma_g^3} \sum_{i=1}^{3}\sum_{j=1}^{3} A_i B_j [g(x_i, y_j) - \mu_g]^3 \tag{19}$$

$$\kappa_g = \frac{1}{\sigma_g^4} \sum_{i=1}^{3}\sum_{j=1}^{3} A_i B_j [g(x_i, y_j) - \mu_g]^4 \tag{20}$$

An earlier study (Au *et al*. 1999) has established that the daily maximum air temperature T_{max} and the daily global solar radiation Q govern the thermal loading during daytime. A correlation analysis (Ho

Table 5 Results of extreme analysis of box girder section for summer condition

Statistical parameters	Max. effective temperature T_e (°C)	Max. top surface temperature T_s (°C)	Extreme positive temperature diff. ΔT (°C)	Max. thermal moment M_T (°C/m)
Mean μ	33.45	42.54	10.09	4.38
Standard deviation σ	0.38	1.08	1.06	0.43
Skewness θ	0.86	1.06	1.10	0.22
Kurtosis κ	4.40	5.16	5.26	4.26
Scale parameter a_n	3.37	1.19	1.22	3.00
Location parameter u_n	33.28	42.06	9.61	4.18
Predicted value y_{50}	34.44	45.33	12.82	5.48
Predicted value y_{120}	34.70	46.07	13.55	5.78

Table 6 Results of extreme analysis of box girder section for winter condition

Statistical parameters	Min. effective temperature T_e (°C)	Min. top surface temperature T_s (°C)	Min. interface temperature T_i (°C)	Max. thermal moment M_T (°C/m)
Mean μ	7.02	7.36	10.73	1.46
Standard deviation σ	1.51	1.23	1.03	1.00
Skewness θ	-1.21	-1.06	-0.57	0.92
Kurtosis κ	5.51	5.29	4.65	5.08
Scale parameter a_n	0.85	1.04	1.25	1.29
Location parameter u_n	6.33	6.81	10.27	1.01
Predicted value y_{50}	1.73	3.06	7.14	4.04
Predicted value y_{120}	0.69	2.21	6.44	4.73

and Liu 1989) between $T_{\max}$ and Q using data of 26 years (1958-62, 1964-84) indeed shows they are effectively uncorrelated, with a correlation coefficient of 0.215. Therefore the application of the above approach is acceptable. The thermal loading F_i considered include the top flange temperature T_s, temperature difference ΔT which is defined as the difference between the highest and lowest temperatures within the section, effective temperature T_e and thermal moment M_T given by

$$M_T = \int TyE\alpha dA / \int y^2 E\alpha dA \tag{21}$$

The estimation of extreme thermal loading during daytime requires bivariate numerical integration using Eqs. (17)-(20) and altogether 9 (i.e., 3×3) combinations of $T_{\max}$ and Q are necessary. For each combination, analysis is carried out on a typical section for summer condition using the parameters in Table 3 and the climatic factors described by Eqs. (11)-(12). The evaluated statistical parameters for each thermal loading are shown in Table 5. The predicted values of thermal loading for return periods of 50 and 120 years are also included.

However the extreme thermal loading during nighttime is essentially governed by the daily minimum air temperature $T_{\min}$ during winter condition and univariate numerical integration suffices. Table 6 shows the evaluated statistical parameters and predicted values for each thermal loading for winter condition.

9. Design temperature profiles

To generate design temperature profiles for general use, only the more important parameters are considered. Design profiles predicted for different thicknesses of bituminous surfacing and concrete slab are given. A fifth-order polynomial (Priestley 1978, AUSTROADS 1992) is used to model the distribution of temperature during daytime. It is assumed that the web will approach the ambient air temperature if it is deep enough. The profile is given by

$$T = \begin{cases} T_D(1-h/h_0)^5 + T_b & 0 \le h \le h_0 \\ T_b & h > h_0 \end{cases} \tag{22}$$

where T is the temperature at a depth h from the top, h_0 is the depth below which the web temperature becomes a constant value T_b, T_D is the difference between the top flange temperature and the constant temperature T_b. Then the values of the parameters T_D, T_b and h_0 are determined so that the fifth-order profile generates the 50-year return values of positive temperature difference ΔT, top surface temperature T_s and thermal moment M_T.

When the parameters T_D, T_b and h_0 are calculated based on the extreme thermal loading, the corresponding extreme temperature profile can be defined. Fig. 10 shows the temperature profile calculated based on the thermal loads of 50-year return period shown in Table 5. The calculated profile is compared with those given in the SDMHR code (HyD 1997), BS5400 (BSI 1978), and those by AUSTROADS (1992) and AASHTO (1998) by aligning the profiles at the soffit. It is observed that, in general, the calculated profile is close to other specifications except the local SDMHR code, which tends to overestimate the temperature especially at the top.

Fig. 11 shows the positive and reverse temperature profiles adopted by the local SDMHR code. For the case of the positive temperature difference, if the values of T_1 to T_2 are chosen according to the fifth-

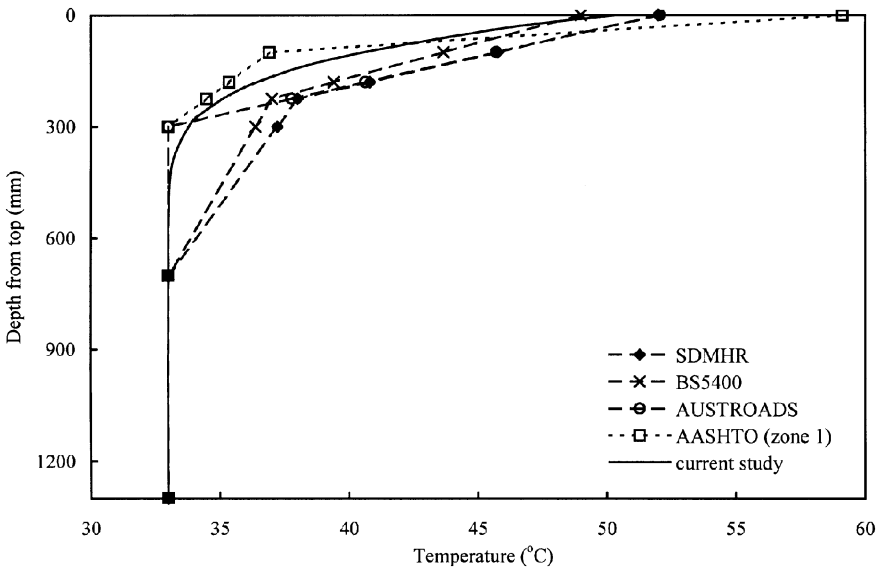

Fig. 10 Design temperature profiles for positive gradient for box girder

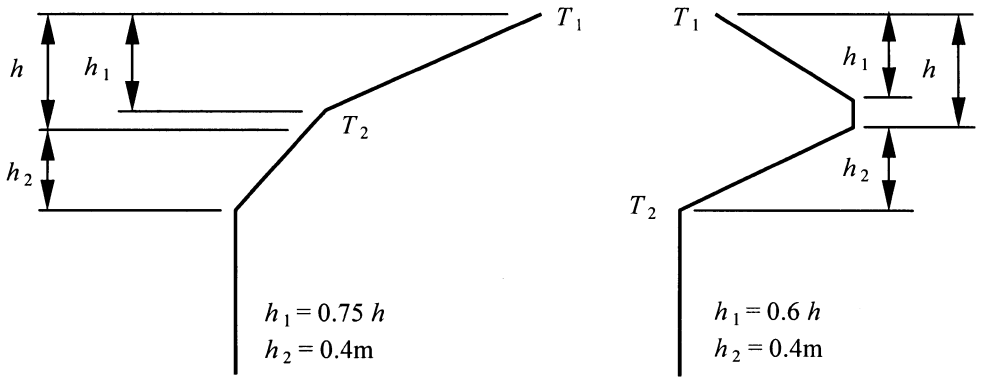

(a) Positive temperature difference (b) Reverse temperature difference

Fig. 11 Design temperature profiles for Group 3 according to Structures Design Manual for Highways and Railways (HyD 1997)

order polynomial, a fairly accurate representation is obtained. Table 7 shows the values of T_1 and T_2 for different thicknesses of surfacing and concrete slab and a 50-year return period, assuming the same values of h_1 and h_2 are maintained.

During nighttime, heat escapes more quickly from the top of concrete slab as well as the supporting steel girders. A single fifth-order polynomial is therefore not sufficient for modelling the temperature profile. Instead two fifth-order polynomials in the form of Eq. (22) are used with one for the concrete slab and another for the steel girders. It is further assumed that the fifth-order polynomial for the concrete slab starts at its interface with the steel girders. Taking into account the continuity property of the temperature profile, the parameters necessary to define the two fifth-order polynomials are the temperature difference $(T_D)_{slab}$ between the top and bottom of the concrete slab, the temperature difference $(T_D)_{girder}$ within the steel girder, and the depth $(h_0)_{girder}$ below which the web temperature becomes a constant value $(T_b)_{girder}$. The three parameters $(T_D)_{slab}$, $(T_D)_{girder}$ and $(h_0)_{girder}$ are determined so that the profile generates the 50-year return values of top surface temperature T_s, interface

Table 7 Positive temperature difference with values from SDMHR (HyD 1997) shown in brackets

Thickness of concrete slab (mm)	Thickness of surfacing (mm)	T_1 (°C)		T_2 (°C)	
200	0	17.15	(17)	6.07	(7)
	40	18.89		6.69	
	50	18.06	(24)	6.40	(12)
	100	15.22	(19)	5.39	(11)
	200	12.13	(13)	4.29	(9)
300	0	17.49	(17)	2.09	(3)
	40	20.74		2.48	
	50	19.80	(24)	2.37	(6)
	100	17.30	(19)	2.07	(5)
	200	12.47	(13)	1.49	(5)

Table 8 Reverse temperature difference with values from SDMHR (HyD 1997) shown in brackets

Thickness of concrete slab (mm)	Thickness of surfacing (mm)	T_1 (°C)		T_2 (°C)	
200	0	3.54	(5)	3.05	(9)
	40	3.11		3.51	
	50	2.99	(3)	3.61	(9)
	100	1.95	(1)	3.75	(9)
	200	1.26	(1)	3.92	(9)
300	0	6.11	(7)	6.20	(9)
	40	5.21		6.49	
	50	4.99	(5)	6.56	(9)
	100	3.96	(4)	6.77	(9)
	200	2.60	(2)	6.99	(9)

temperature T_i, and thermal moment M_T as shown in Table 6. The values of T_1 and T_2 at the levels shown in Fig. 11(b) are shown in Table 8 for different thicknesses of surfacing and concrete slab and a 50-year return period. Fig. 12 shows the reverse temperature profile calculated based on the thermal loads of 50-year return period for the box girder shown in Fig. 3. The calculated profile is compared with those given in the other design codes by aligning the profiles at the interface between concrete slab and steel girder. It is seen that apart from the AASHTO (1998) code which ignores the temperature gradient within the steel girders, all other codes specify separate temperature gradients for the concrete slab and steel girders. The calculated profile is close to most code specified profiles with the exception of the AASHTO (1998) profile.

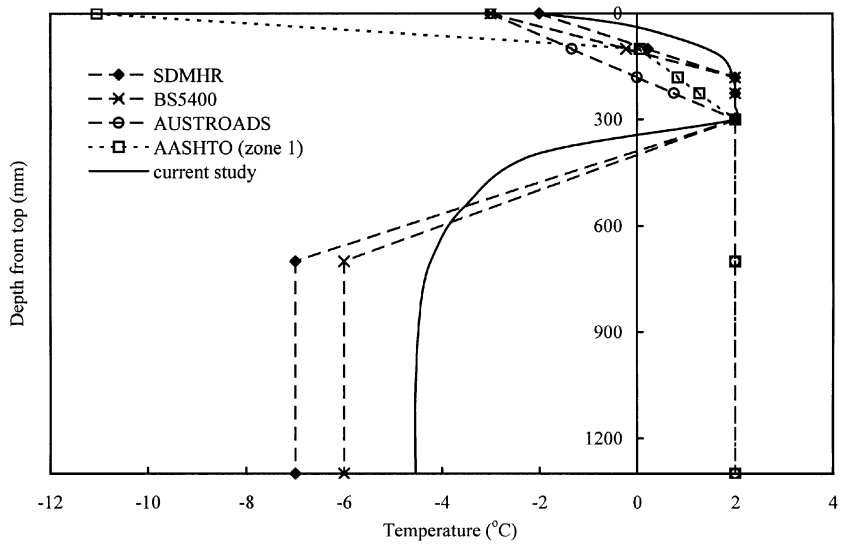

Fig. 12 Design temperature profiles for reverse gradient for box girder

10. Design effective temperatures

Using the results from the extreme analysis, the extreme effective temperatures can be calculated from Eq. (1). For a typical composite section as shown in Fig. 3, the effective temperature actually depends primarily on the concrete slab and the contributions from the top flange, the web and the bottom flange of the steel girder. The effective temperature becomes higher with thinner bituminous surfacing and concrete slab. Using the previous results from the extreme analysis, Table 9 summarizes the results for a 50-year return period for different thicknesses of bituminous surfacing and concrete slab, and compared with the recommendations of SDMHR (HyD 1997).

11. Conclusions

After a comprehensive study of the thermal behaviour of composite bridges, it is confirmed that the shade air temperature and solar radiation are the most influential factors affecting their temperature distribution. For bridges of considerable width, the validity of the one-dimensional heat transfer model has been verified. By using mathematical models based on parameters validated by field studies, extreme analysis is carried out based on the statistics of extremes and numerical integration. The method has been applied to typical composite sections comprising a concrete slab supported on plate girders or box girders. Some design temperature profiles have been developed, with allowance for various thicknesses of bituminous surfacing and concrete slab. The design temperature differences and effective temperatures have been obtained and compared to the recommendations of the local code as well as codes in other countries. It confirms that the existing requirements are reasonable. This paper illustrates a systemic approach to the development of site-specific temperature profiles for code documents where the requisite climatic information for a particular geographic location is available. Although this paper describes only its application to Hong Kong, the method can also be applied to create zoning maps for temperature loading for large countries where there are great climatic differences.

Table 9 Design effective temperatures for a 50-year return period with values from SDMHR (HyD 1997) shown in brackets

Thickness of concrete slab (mm)	Thickness of surfacing (mm)	Minimum effective temperature (°C)		Maximum effective temperature (°C)	
0.2	0	-0.18	(-3)	37.50	(38)
	40	0.29	(-2)	37.42	(40)
	50	0.39		37.07	
	100	0.81	(0)	35.66	(38)
	200	1.39	(3)	34.27	(34)
0.3	0	0.93	(-3)	36.40	(38)
	40	1.31	(-2)	36.26	(40)
	50	1.40		36.01	
	100	1.73	(0)	35.03	(38)
	200	2.18	(3)	33.60	(34)

References

American Association of State Highway and Transportation Officials (1996), *Standard Specifications for Highway Bridges*, 16th ed., Washington, D.C., U.S.A.

American Association of State Highway and Transportation Officials (1998), *AASHTO LRFD Bridge Design Specifications*, 2nd ed., Washington, D.C., U.S.A.

Au, F.T.K., Tham, L.G. Tong, M., (2001), "Design thermal loading for steel bridges in Hong Kong", *HKIE Transactions*, **8**(2), August, 1-9.

Au, F.T.K., Tham, L.G., Tong, V.M. and Lee, P.K.K. (1999), "An initial review of design thermal loading for bridges in Hong Kong", *Proc. of Seminar of Structural Aspects of Airport Core Program Projects*, 7 May, 89-103.

AUSTROADS (1992), *Bridge Design Code: Section 2 - code and commentary*, Sydney.

British Standard Institution (1978), *BS5400, Steel, Concrete and Composite Bridges*, London, U.K.

Capps, M.W.R. (1968), *The Thermal Behavior of the Beachley Viaduct/Wye Bridge*, Ministry of Transport, Road Research Laboratory, RRL Rep. LR 234.

Cheung, S.K. (2002), *Review of Local Design Code on Temperature Distribution in Composite Bridges*, M.Sc.(Eng.) Dissertation, The University of Hong Kong, Hong Kong.

Emerson, M. (1968), *Bridge Temperatures and Movements in the British Isles*, Ministry of Transport, TRRL Rep. LR 228.

Emerson, M. (1973), "The calculation of the distribution of temperature in bridges", Department of the Environment, TRRL Rep. LR 561.

Emerson, M. (1976), "Bridge temperatures estimated from the shade temperature", Department of the Environment, TRRL Rep. LR 696.

Evans, D.H. (1972), "An application of numerical integration techniques to statistical tolerencing III - General distribution", *Technometrics*, 14.

Gumbel, E.J. (1960), *Statistics of Extremes*, Columbia University Press, New York.

Highways Department (1997), *Structures Design Manual for Highways and Railways*, 2nd ed, Hong Kong Government.

Hirst, M.J.S. (1981), "Solar heating of bridges", *Australian Road Research Board,* **11**(2), June, 28-36.

Ho, D. and Liu, C.H. (1989), "Extreme thermal loadings in highway bridges," *J. Struct. Div.,* ASCE, **115**(7), July, 1681-96.

Hunt, B. and Cooke, N. (1975), "Thermal calculations for bridge design", *J. Struct. Div.,* ASCE, **101**, September, 1763-81.

Kennedy, J.B. and Soliman, M.H. (1987), "Temperature distribution in composite bridges", *J. Struct. Eng.,* **113**(3), March, 475-82.

Liu, C.H. (1985), "Investigation of temperature distribution in highway bridges", M.Phil. Thesis, The University of Hong Kong, Hong Kong.

Ministry of Transport (1991), Canada, *Ontario Highway Bridge Design Code and Commentary*, 3rd ed.

Priestley, M.J.N. (1978), "Design thermal gradient for concrete bridges", *New Zealand Engineering,* **31**(9), 213-219.

Reynolds, J.C. and Emanuel, J.H. (1974), "Thermal stresses and movements in bridges", *J. Struct. Div.*, ASCE, **100**, January, 63-78.

Tong, M.V. (2000), "Temperature distribution in highway bridges", M.Phil. Thesis, The University of Hong Kong, Hong Kong.

Tong, M., Au, F.T.K., Tham, L.G. and Wong, K.Y. (2000), "A study of temperature measurement in long span steel bridge", *Proc. of Workshop on Research and Monitoring of Long Span Bridges*, The University of Hong Kong, 26-28 April, 188-195.

Tong, M., Tham, L.G., Au, F.T.K. and Lee, P.K.K. (2001), "Numerical modelling for temperature distribution in steel bridges", *Computers and Structures*, **79**(6), February, 583-593.

Yik, F.W.H., Chung, T.M. and Chan, K.T. (1995), "A method to estimate direct and diffuse radiation in Hong Kong and its accuracy", *HKIE Transactions*, **2**(1), 23-29.

Zuk, W. (1965), "Thermal behaviour of composite bridges - insulated and uninsulated", *Highway Research Record*, No. 76, 231-253.

CC